

Buckling and post-buckling behaviors of 1/3 composite cylindrical shell with an opening

Yihao Ma^{1a}, Xiaoquan Cheng^{*1,2}, Zhaodi Wang³, Xin Guo¹, Jie Zhang¹ and Yahong Xu³

¹ School of Aeronautic Science and Engineering, Beihang University, Beijing, 100191, China

² Key Laboratory of Aircraft Advanced Design Technology (Beihang University),
Ministry of Industry and Information Technology, Beijing, 100191, China

³ Institute 306 of the 3rd Academy of CASIC, Beijing, 100074, China

(Received November 28, 2017, Revised March 15, 2018, Accepted March 28, 2018)

Abstract. A 1/3 composite cylindrical shell with a central rectangular opening was axially compressed experimentally, and its critical buckling load and displacement, and strains were measured. A finite element model (FEM) of the shell with Hashin failure criteria was established to analyze its buckling and post-buckling behaviors by nonlinear Newton-Raphson method. The geometric imperfection sensitivity and the effect of side supported conditions of the shell were investigated. It was found that the Newton-Raphson method can be used to analyze the buckling and post-buckling behaviors of the shell. The shell is not sensitive to initial geometric imperfection. And the support design of the shell by side stiffeners is a good way to obtain the critical buckling load and simplify the experimental fixture.

Keywords: composite shell; opening; post-buckling; Newton-Raphson method; FEM; axial compression

1. Introduction

Composite materials are widely used in flight vehicles because of their high specific strength and modulus, performance designability and other advantages. Missile and rocket bodies, helicopter rear fuselages and other key structures are usually designed and manufactured as composite cylindrical shells (Ye *et al.* 2011, Reddy *et al.* 2015). Due to the installation of equipment inside the shell, as well as the routine inspection and maintenance, it usually needs openings and covers on the shell. For missiles and rockets, axial compression is a critical loading condition, and buckling failure occurs easily in the thin-walled shell structures of their bodies instead of static compressive strength failure. So it is important to study the buckling and post-buckling behaviors of composite cylindrical shell under axially compressive load.

Many studies have been carried out on the buckling and post-buckling behaviors of cylindrical shell structures. They were commonly conducted by experimental and theoretical methods, in which the theoretical investigation includes analytical and numerical methods. Analytical method is suitable for simple structures and load conditions (Dong *et al.* 2017, Aragh 2017, Mahmoud and Tounsi 2017, Shokravi 2017), while finite element method is usually used for complex structures (Akbas 2017, Dubina *et al.* 2005, Altunisik *et al.* 2017). Jabareen and Sheinman (Sheinman and Jabareen 2005, 2006, 2007, Jabareen 2009) conducted

many studies on the buckling and post-buckling behaviors of cylindrical and conical shells. It was found that post-buckling analysis can obtain the entire load-displacement curves under dynamic step loading, and the cylindrical/conical shells are sensitive to initial geometric imperfections. Spagnoli and Chryssanthopoulos (1999) analyzed the linear elastic buckling and nonlinear post-buckling behaviors of thin cylindrical/conical shells with stiffeners under axially compressive load, and they found the stiffening spacing influences the imperfection sensitivity of cylindrical/conical shells. Li *et al.* (1995) studied the effect of thickness variation on the stability of composite cylindrical shells under axial compression. The results show that some thickness variation patterns can greatly reduce the classical buckling load, and the most detrimental effect of the thickness variation occurs when the wave number of the thickness variation is twice that of the classical buckling mode. Based on the classical shell theory and von Karman-Donnell type of kinematic nonlinearity, Li and Qiao (2015) developed a boundary layer theory to study the buckling and post-buckling properties of anisotropic laminated cylindrical shells under combined external pressure and axial compression. They found that there exists a circumferential stress or a compressive stress along with an associate shear stress, and the shear stress will affect the buckling load and post-buckling behavior of the shell. Arbelo *et al.* (2015a) developed a numerical model based on the vibration correlation technique (VCT) to predict the buckling loads of cylindrical shells under compression. All of above studies were carried out on complete structures without any openings.

Jullien and Limam (1998) studied the effect of opening on buckling and post-buckling behaviors of cylindrical

*Corresponding author, Professor,
E-mail: xiaoquan_cheng@buaa.edu.cn
^a Ph.D., E-mail: mayihao@buaa.edu.cn

shells under axial compression by experimental and numerical methods. The influence of the shape, size, position and quantity of the openings were studied. Hilburger and Starnes (2002) studied the effects of initial imperfections on the buckling and post-buckling response of unstiffened thin-walled compression-loaded composite cylindrical shells with different orthotropic and quasi-isotropic laminates by experimental and numerical methods. They found that the buckling loads of the orthotropic shells are less sensitive to the imperfections than that of the quasi-isotropic shells. Later, they (Hilburger and Starnes 2005) numerically studied the response of quasi-isotropic laminated composite cylindrical shells with unreinforced and reinforced square cutouts under compressive load. The results show that for a shell with an unreinforced cutout, a local buckling response occurs in the shell near the cutout, which is caused by a complex non-linear coupling between local out-of-plane deformations and in-plane destabilizing compressive stresses near the cutout. Besides, reinforcement around the cutout can increase the buckling load of the shell, but certain reinforcement configurations can cause an unexpected increase in the magnitude of local deformations and stresses in the shell and reduce the buckling load. They (Hilburger *et al.* 1999) also investigated the similar composite cylindrical shells with cutouts under axially compressive load and internal pressure. The results show that the size of the cutouts and the internal pressure load can affect the local load distributions and displacements near the cutout, and then result in local buckling. Tafreshi (2002) conducted a similar research by numerical method, and the results show that the critical buckling load of cylindrical shells decreases with the opening size increasing or internal pressure decreasing. When the opening area keeps the same, the larger axial dimension causes the smaller critical buckling load. Taheri-Behrooz *et al.* (2017) employed experimental and numerical procedures to investigate the effects of initial geometric imperfection on the buckling behaviors of perfect and perforated composite cylinders. The results show that the cutout is the dominant factor which affects compressive behavior of the cylinder with a cutout, while initial geometric imperfection has a negligible effect on the buckling load. Yan *et al.* (2012) and Wu *et al.* (2014) investigated the axial compression behavior of composite cylindrical shell with an opening by experimental and finite element methods. They only calculated the critical buckling load by linear eigenvalue method without analyzing the post-buckling behavior of the structure. Arbelo *et al.* (2015 b) investigated the effects of a cutout on the buckling load of a thin-walled curved panel and a cylindrical shell, they found that the buckling load of cylindrical shells with a cutout is strongly affected by the cutout diameter, but after a given threshold diameter it remains nearly constant. Furthermore, when the Single Perturbation Load Approach (SPLA) is applied in cylindrical shells with a cutout, the initial geometric imperfection generated by the perturbation load is dominant for smaller cutout size. But for bigger cutout size, the imperfection generated by the cutout is dominant and the effect of the SPLA is negligible in the knock-down factor. Knight and Starnes (1985) experimentally studied the post-

buckling behavior of axially compressed graphite-epoxy cylindrical shells with circular holes, in which the influence of circular hole diameter, cylindrical shell radius and thickness was investigated. It was found that the post-buckling response characteristics of the specimens with larger shell radii are similar up to failure regardless of the hole size, while the local deformations near the holes in the specimens with smaller shell radii cause local laminate-related failures, and the hole size influences the post-buckling behaviors of these specimens. Then they conducted a numerical simulation with linear elastic material properties and obtained the post-buckling equilibrium path of the structures, in which no damage was considered. However, local delamination was observed around the hole in the experiment. Orifici *et al.* (2008a, b) and Degenhardt *et al.* (2008) also conducted a lot of research on the post-buckling and damage mechanism of the composite stiffened panels. They developed an analysis method to investigate the collapse in post-buckling composite structures and predict the initiation of inter-laminar damage in skin-stiffener interface, and the predicted failure load and failure mechanisms were close to experimental results. Most of above studies are focused on complete cylindrical shells, but in engineering practice, the specimen is usually fabricated as one part configuration of a complete cylindrical shell to save experimental cost, especially for large-scale structure. Little research has been carried out in this field.

In this paper, a 1/3 composite cylindrical shell with a central rectangular opening was fabricated and compressed experimentally to investigate its buckling and post-buckling behaviors. Based on the experimental results, a FEM of the shell with composite damage criteria was established, and imperfection sensitivity was analyzed. Besides, an unconventional side supported method was proposed and compared with conventional method to verify its feasibility. The analysis method can be applied to analyze the compressive behavior of composite cylindrical shell with an opening, and the results can be used as a reference for the related structure and specimen design.

2. Experimental procedures

2.1 Specimen and materials

The specimen was taken from a composite cylindrical shell with longitudinal and circumferential stiffeners as shown in Fig. 1. In order to save material cost and verify the design analysis method, the typical specimen was designed and fabricated as a 1/3 configuration of the complete cylindrical shell as shown in Fig. 2. The outer radius of the shell is 257 mm, with a height of 608 mm and a thickness of 1.6 mm. There are stiffeners with a width of 10 mm and a thickness of 2 mm at 30° and 90° along circumferential direction, and 196 mm and 392 mm along longitudinal direction respectively, resulting to a “#” frame inside the cylindrical shell (Fig. 2(a)). There is a rectangular opening in the centre of the cylindrical shell, with a height of 170 mm and a width of 230 mm. A patch with a thickness of

2.64 mm is attached on the inner surface of the shell to strengthen the opening area with a smaller central rectangular opening which is 120 mm high and 180 mm wide. The patch has free edges with a width of 25 mm around the opening, which are used to install the cover. Both the openings on cylindrical shell and patch have rounded corners with a radius of 15 mm (Figs. 2(a)-(b)). In order to simulate the boundary conditions and reduce the experimental fixtures, both longitudinal sides of the specimen are strengthened by a couple of side stiffeners (Fig. 2(c)), and each side stiffener has a height of 588 mm, a width of 20 mm and a thickness of 8 mm.

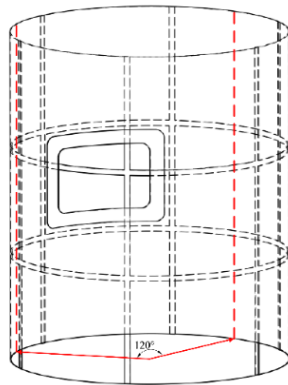
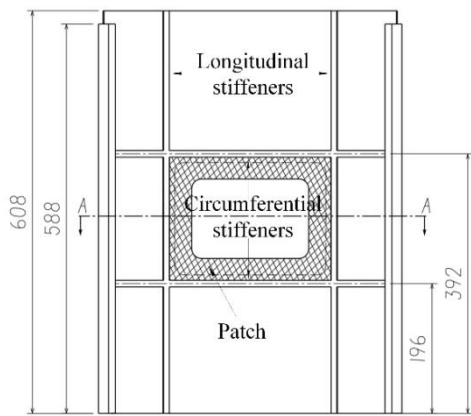


Fig. 1 Entire composite cylindrical shell

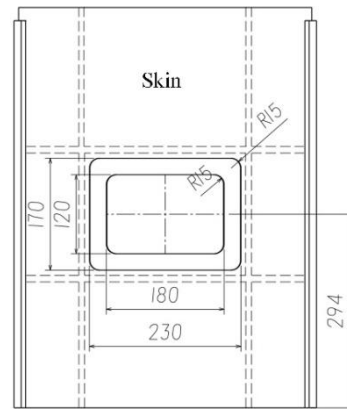
Two kinds of materials of T300/6808 (carbon/epoxy) lamina and G814/6084 (carbon/epoxy) fabric were used in the specimen. The mechanical properties of each material are listed in Table 1. The stacking sequence and material of each part are listed in Table 2. T300/6808 lamina possess two thicknesses involving 0.16 mm and 0.125 mm, in which the 0.16 mm lamina was used in the skin and the

Table 1 Mechanical properties of T300/6808 and G814/6084

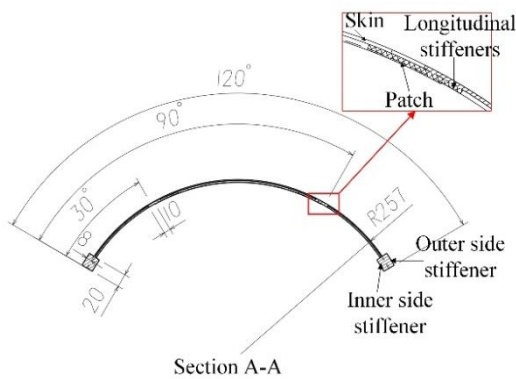
Items	T300/6808	G814/6084
Longitudinal elastic modulus, E_1 (GPa)	117.0	63.0
Transversal elastic modulus, E_2 (GPa)	8.0	63.0
Poisson's ratio, ν_{12}	0.16	0.06
In-plane shear modulus, G_{12} (GPa)	3.00	4.10
Out-plane shear modulus, G_{13} (GPa)	3.00	4.10
Out-plane shear modulus, G_{23} (GPa)	2.00	2.73
Longitudinal tensile strength, X_T (MPa)	1469	856
Longitudinal compression strength, X_C (MPa)	1480	800
Transversal tensile strength, Y_T (MPa)	27	856
Transversal compression strength, Y_C (MPa)	245	800
In-plane shear strength, S_L (MPa)	98	95
Out-plane shear strength, S_T (MPa)	98	95



(a) Inner view



(b) Outer view



(c) Section view of A-A



(d) The specimen

Fig. 2 Geometrical dimensions of the specimen

Table 2 Stacking sequences and materials of different parts of the specimen

Part	Material	Layer thickness	Stacking sequence	Layer number
Skin	T300/6808	0.160 mm	$[45/-45/0_2/90]_S$	10
Longitudinal stiffener	T300/6808	0.125 mm	$[45/-45/0_2/45/-45/0/90]_S$	16
Circumferential stiffener	T300/6808	0.125 mm	$[-45/45/90_2/-45/45/90/0]_S$	16
Side stiffener	T300/6808	0.125 mm	$[45/-45/0_2/45/-45/0/90_2/0/-45/45/0_2/-45/45]_{2S}$	64
Patch	G814/6084	0.240 mm	$[0_{11}]$	11

0.125 mm one was used in all the stiffeners. The specimen was fabricated by Resin Transfer Molding (RTM) process. The specimen is shown in Fig. 2(d).

2.2 Test procedures

The experiment was carried out in an Instron 8803 test machine (500 kN servo-hydraulic test machine). A special fixture was designed and used to clamp the upper and lower ends of the shell, which restrains its radial deformation, makes its axial displacement uniform and prevents the ends from crushing. The lower fixture is shown in Fig. 3. The upper fixture is similar to the lower one, except that there is no slot for side stiffeners in both base and slider. The fixture and loading condition of the specimen are shown in Fig. 4.

Firstly, the specimen was axially pre-compressed twice with a load of 7 kN to eliminate the gap between the fixture and the specimen, and then the load was applied step by step until the specimen failed. The load increment was 10 kN when the load was less than 50 kN, while the increment was 5 kN when the load exceeded 50 kN. The strain gauges were attached at some positions as shown in Fig. 5, in which the numbers with brackets denote the gauges that

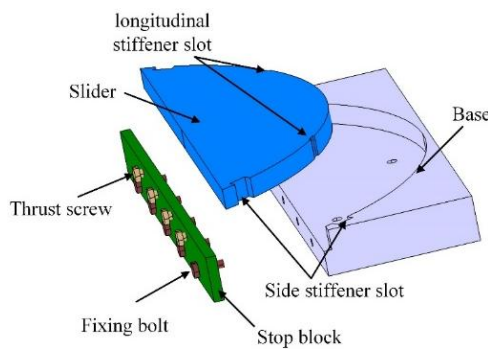


Fig. 3 Schematic diagram of the lower fixture

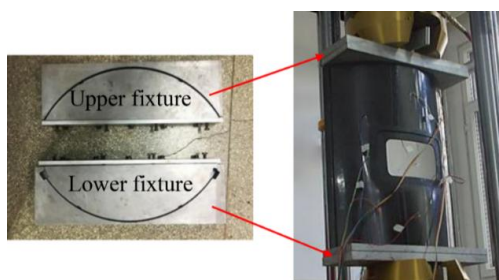


Fig. 4 Fixture and loading condition of the specimen

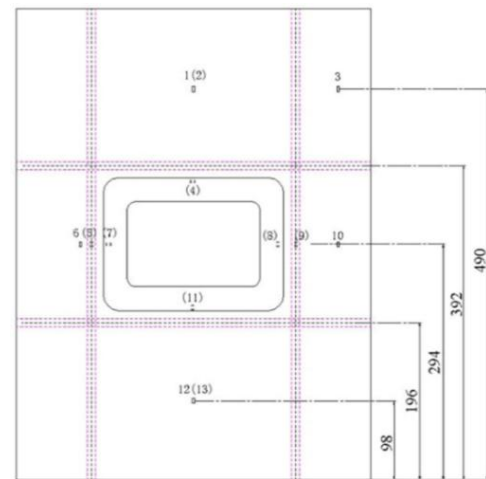
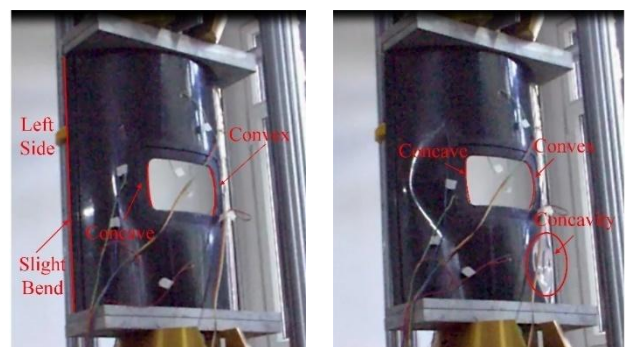


Fig. 5 Strain gauge positions on the specimen

are attached to the opposite side of the shell. The load and corresponding strain were recorded.

2.3 Experimental results

The main purpose of the experiment was to obtain the critical buckling load and buckling mode of the 1/3 composite cylindrical shell with an opening. No obvious deformation occurred in the initial stage of loading. As the load increasing to about 35 kN, radial deformation occurred at both sides of the opening with right side convex outward and left side concave inward, and the sides of the shell slightly bent as shown in Fig. 6(a). When the load and displacement reached 65.9 kN and 0.75 mm respectively, a large deformation occurred in the specimen suddenly with a



(a) At 35 kN (b) At the failure load

Fig. 6 Deformation of specimen



Fig. 7 Cracks close to upper end of the specimen

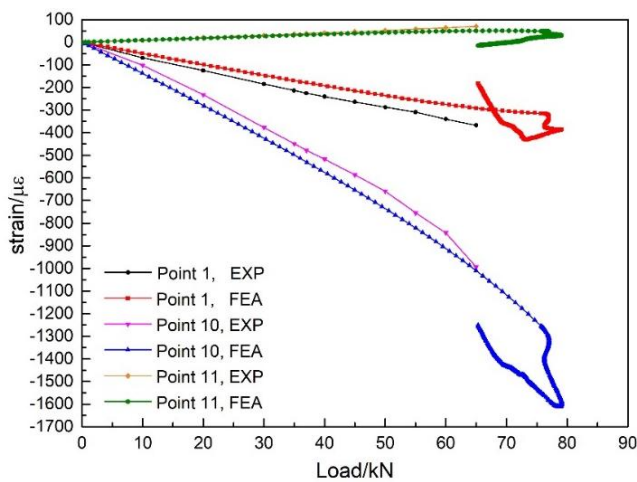


Fig. 8 Experimental and numerical strain-load curves at Point 1, 10 and 11

loud noise. The left side of the opening was concave inward deeply and the right side was convex outward seriously, and a concavity occurred in the lower right corner of the shell at the same time, as shown in Fig. 6(b), which is a critical buckling load state. For the displacement of crosshead increased to the assigned limit value, the experiment stopped. During the unloading process, all the deformations in the shell bounced back to the original shape. Matrix damage, cracks and small local delamination were observed close to the upper ends of the side stiffeners as shown in Fig. 7. The strain-load curves of three typical positions (point 1, 10 and 11) are shown in Fig. 8.

3. Numerical modeling

A FEM of the 1/3 composite cylindrical shell with an opening under axial compressive load was established by ABAQUS 6.13. Firstly, the linear eigenvalue buckling analysis of the shell was carried out to obtain the critical buckling loads and buckling modes. Secondly, initial geometric imperfection was introduced to the model and nonlinear buckling analysis was conducted to investigate its nonlinear buckling and post-buckling behaviors.

There are three methods in ABAQUS to introduce initial

geometric imperfections into the model (Abaqus-inc. 2013): (1) by linearly superposing the buckling eigenmodes obtained from a previous eigenvalue buckling analysis; (2) by adding the displacement obtained from static analysis; (3) by specifying node defects directly. In theory the third method is most accurate, but in practice it is difficult to accurately detect and define the initial defects of the structure. In most cases, the first method is a reasonable way to estimate the imperfect geometry, so it was employed here.

The initial geometric imperfection is defined as

$$\omega = \mu h \times \text{linear buckling mode} \quad (1)$$

Where μ represents the imperfection coefficient and h represents the shell thickness. In general, μ is taken as a few percent of the shell thickness.

3.1 Finite element model

The thickness of the shell is 1/335 to its circumferential length, so the structure can be considered to be a thin shell. The reduced integrated S4R shell element was used in the FEM, which is particularly suitable for geometrical nonlinear problems because it involves finite membrane strains, large rotations and the effect of shear deformations. In this model, the skin, patch and all the stiffeners were separately built according to the materials and stacking sequences in Tables 1 and 2 by composite layup method, as shown in Fig. 9(a). Then all parts were combined into an integral assembly by tie constraints. The mesh size of the FEM was set to 4 mm, and was refined in the region of the shell upper end close to the side stiffener tips where great stress concentrations maybe occur, as shown in Fig. 10. The total number of the mesh is 25788. Fixed constraints were applied to the nodes within 15 mm range from the top of the shell, while the axial translation freedom of the nodes within 15 mm range from the bottom was free and all other freedoms were fixed. Multi-point constraint (MPC) was established between the nodes on the specimen lower end and a central reference point (RP) to keep the axial displacements uniform. The specimen FEM is shown in Fig. 9(b), in which U_i ($i = 1, 2$) represents the translational degree of freedom (DOF) along the cylindrical coordinate axes i , and UR_j ($j = 1, 2, 3$) represents the rotational DOF around the axes j .

3.2 Linear eigenvalue buckling analysis

Firstly, a compressive load of 1.0 kN was applied to the RP of MPC and linear eigenvalue buckling analysis was carried out to obtain the first-order buckling load and buckling modes. The first-order buckling load is 88.79 kN, and some buckling modes are shown in Fig. 11 with an amplification factor of 50. The deformation contour represents the deformation in radial direction (1 direction) with red colour indicating convex outward and blue colour concave inward. It can be seen that the lower order modes (Mode 1 and 2) are local deformation around the opening and the higher order modes (Mode 12, 17 and 20) are global deformation. These buckling modes will be used as the

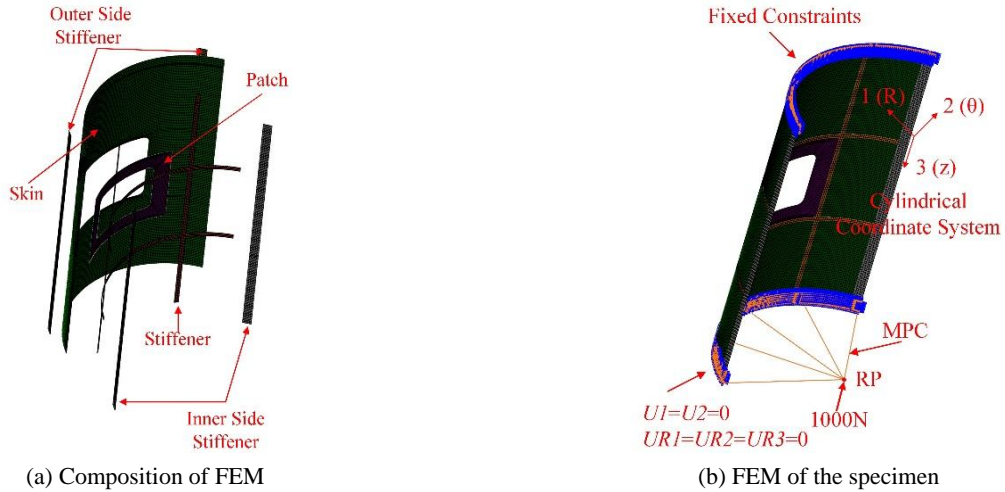


Fig. 9 FEM of the 1/3 composite cylindrical shell with opening

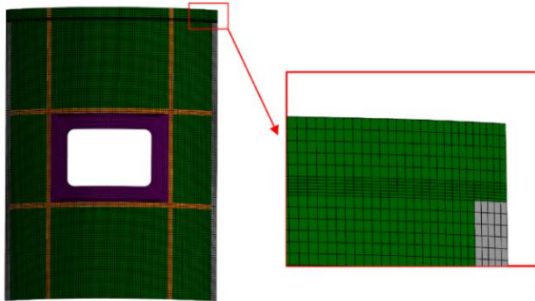


Fig. 10 The FEM mesh

initial geometric imperfections in the nonlinear buckling analysis later.

Comparing buckling mode 1 with the experimental buckling deformation, it is found that two buckling modes are not consistent, though both the deformations locate at the edges of the opening. The numerical critical buckling load is 88.79 kN which is 34.7% greater than experimental result. Therefore, the linear eigenvalue buckling analysis is inapplicable to predict the critical buckling load and mode of the 1/3 composite cylindrical shell with an opening. This is because the linear eigenvalue buckling analysis is based on the original shape and stiffness of the structure, without

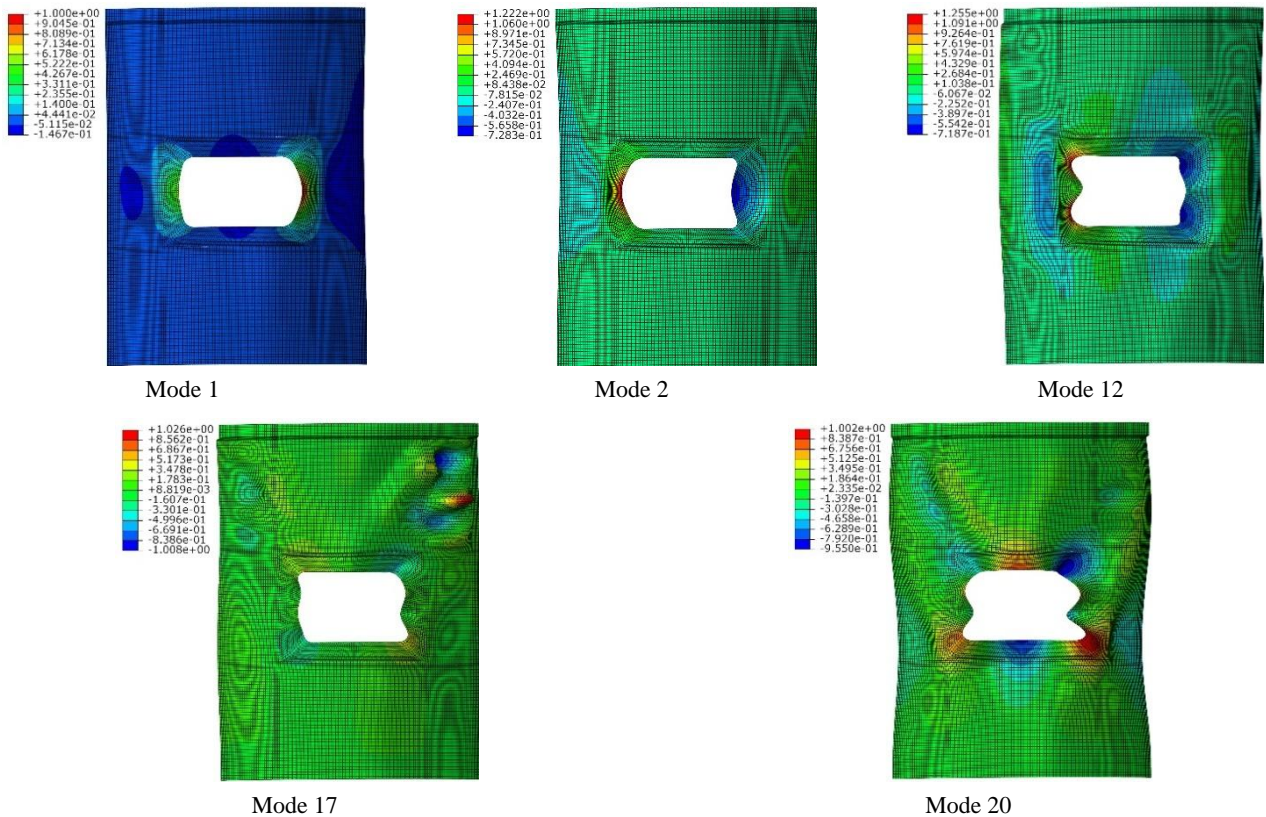


Fig. 11 Buckling eigenmodes of the model

considering geometric imperfections and stiffness change caused by structure deformation and damage in the loading process. But it can obtain the buckling mode of the structure to some extent. For the same shell without opening, the linear eigenvalue buckling method can give accurate critical buckling load and mode because the structure is almost symmetric (Li *et al.* 2011). But the opening causes stiffness mutation and structural asymmetry of the shell and leads to large out-of-plane deformation around it at a small load. So the geometric nonlinear should be considered here.

3.3 Nonlinear buckling and post-buckling analysis

Three methods can be used for nonlinear buckling analysis: explicit dynamic method, Newton-Raphson method and Riks method. For explicit dynamic method, structure buckling is considered as a quasi-static phenomena (Lanzi and Giavotto 2006), so the loading time should be long enough to eliminate dynamic effects, otherwise it could overestimate the buckling load. The loading time used here is more than 2 second, and the corresponding computing time on a machine with 8 CPU cores is more than 12 hours which is too long to be adopted. For Riks method, it is difficult to keep the stability and convergence of the calculation when geometric and material non-linearity is involved. Besides, the calculated load-displacement curve is influenced by the initial load (see Fig. 12) which is difficult to be selected. Therefore, this method was also discarded. The Newton-Raphson method turned out to be applicable and had a good convergence for this model, so it was employed here to analyse the compressive behaviour of the shell.

Damage may occur in the composite shell while the load increases to some value, so the failure criteria based on Hashin and Rotem's (1973) theory were employed to predict the damage. The criteria include four different damage forms, which are fiber tension, fiber compression, matrix tension and matrix compression. Delamination damage was not taken into account because stress in the thickness direction cannot be obtained by S4R shell element. A brief description of the failure criteria (Eqs. (2)-(5)) is shown as followings.

Fiber tension ($\sigma_{11} \geq 0$)

$$\left(\frac{\sigma_{11}}{X_T}\right)^2 \geq 1 \tag{2}$$

Fiber compression ($\sigma_{11} < 0$)

$$\left(\frac{\sigma_{11}}{X_C}\right)^2 \geq 1 \tag{3}$$

Matrix tension ($\sigma_{22} \geq 0$)

$$\left(\frac{\sigma_{22}}{Y_T}\right)^2 + \left(\frac{\tau_{12}}{S_L}\right)^2 \geq 1 \tag{4}$$

Matrix compression ($\sigma_{22} < 0$)

$$\left(\frac{\sigma_{22}}{2S_T}\right)^2 + \left[\left(\frac{Y_C}{2S_T}\right)^2 - 1\right] \frac{\sigma_{22}}{Y_C} + \left(\frac{\tau_{12}}{S_L}\right)^2 \geq 1 \tag{5}$$

Where σ_{ii} and τ_{ij} ($i, j = 1, 2$) denote normal and shear stress components respectively. X_T and X_C represent longitudinal tensile and compressive strength respectively. Y_T and Y_C represent transversal tensile and compressive strength respectively. S_L and S_T represent in-plane and out-plane shear strength.

The first few buckling modes are frequently considered to provide the most critical imperfections of the structure. These modes are amplified with a factor and superposed to form an initial perturbation to the shell. In this paper, the first order eigenmode obtained from previous linear eigenvalue buckling analysis was introduced to the FEM as the initial geometric imperfection with an amplification factor of 0.264 that means 10% of the patch thickness. The FEM of the imperfect 1/3 cylinder shell is shown in Fig. 13. The MPC between the nodes on the specimen lower end and RP was replaced by kinematic coupling constraints, and all freedoms except the axial translation freedom of the RP were constrained. The compressive load on RP was removed and an axial compressive displacement of 1.2 mm was applied to it. The compressive load was obtained by extracting the reaction force on the fixed end.

The load-displacement curve of the 1/3 composite cylindrical shell is shown in Fig. 14. It can be seen that the curve remains straight at the initial stage, which indicates the structural stiffness remains constant. Then the curve

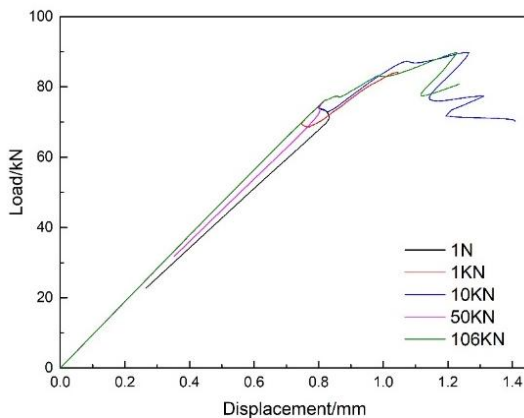


Fig. 12 Load-displacement curves by Riks method with different initial loads



Fig. 13 Mesh with the geometric imperfection amplified with a factor of 200

reaches the first maximum point A with the value of 77.02 kN which is taken as the nonlinear critical buckling load. Its relative error is 16.87% compared with the experimental value. This result is more accurate than that by previous linear eigenvalue buckling analysis. As the specimen cannot be fabricated and tested ideally, it is reasonable that the numerical result is higher than the experimental result. The deformation of the shell corresponding to point A is shown in Fig. 15 which shows the deformations mainly occur at the opening edges and shell sides, and the maximum deformation is 1.633 mm which is very small relative to the shell radius. The deformation is similar to the experimental result before buckling.

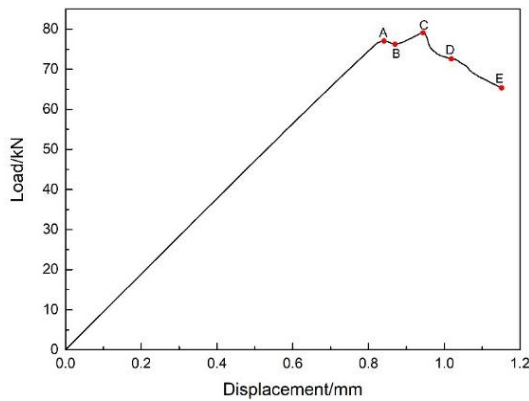


Fig. 14 Load-displacement curve obtained by nonlinear buckling analysis

The numerical strain-load curves of point 1, 10 and 11 are compared with the experimental results in Fig. 8. It shows that the FEM results are in good agreement with the experimental results before the critical buckling load of point A.

Fig. 15 shows the deformation of the shell corresponding to point A to E on the load-displacement curve (Fig. 14). Following point A, the load decreases to point B (see Fig. 14), which represents the buckling process. Then, the curve rebounds to point C with a maximum load of 79.09 kN, which represents the post-buckling behavior of the shell. It can be seen from Fig. 15 that the deformations of the shell from point A to C change little. After point C, the load drops rapidly and never increases again, which represents the shell collapsed. It can be seen a concavity occurs in the upper left corner of the shell at point D and then changes to the deformation of point E. The shell deformation of point E is close to the experimental result except that the concavity is in the upper left corner instead of the lower right corner of the shell. The concavities in two diagonal corners are symmetrical about the center of the shell, and the location difference between the experimental and numerical results is reasonable because the shell is basically symmetric.

In the experiment process, the specimen collapsed directly after buckling without realizing its post-buckling potential. This may relate to the serious damage at the upper end caused by the buckling deformation (see Fig. 7). In FEA result, the fiber tension damage and matrix damage initiate at left side close to the upper end around point A,

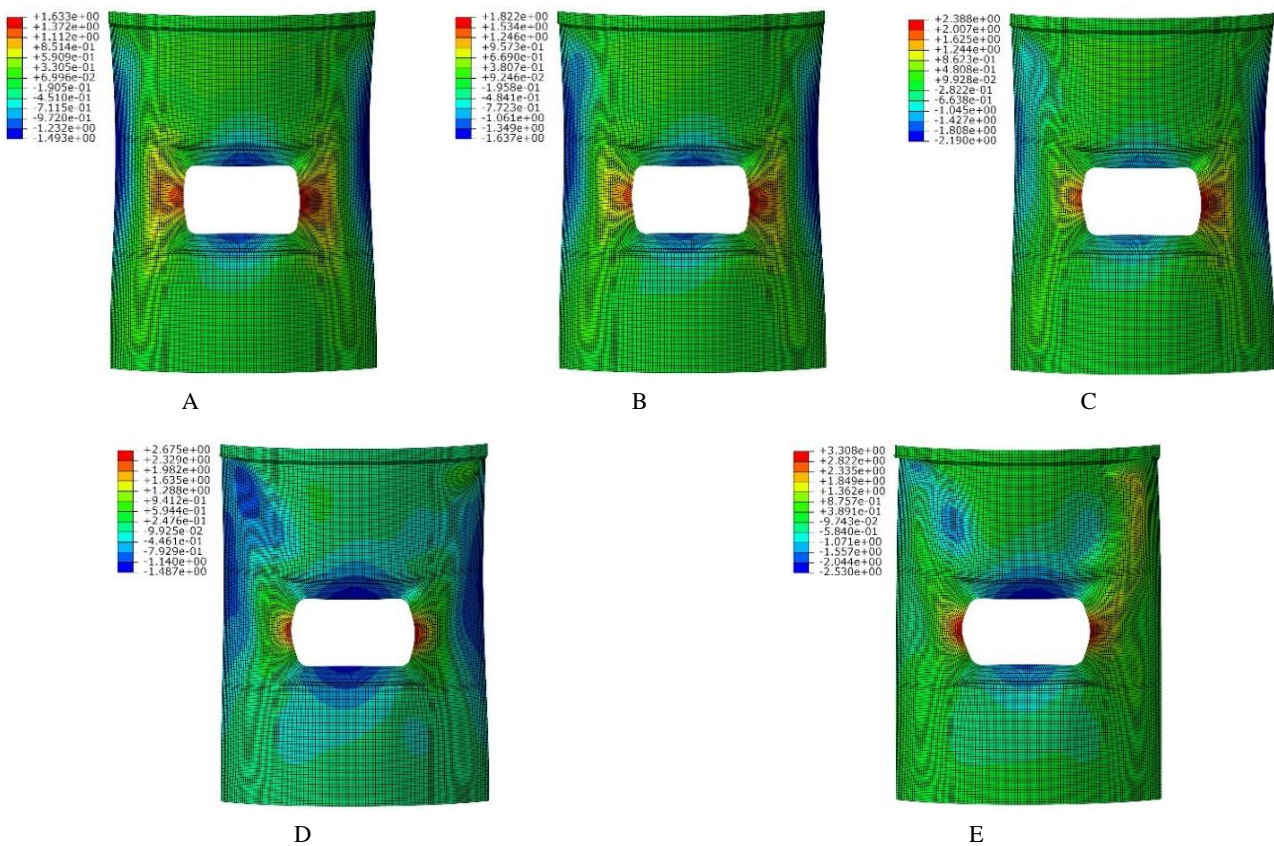


Fig. 15 Deformations of the shell corresponding to point A~E with amplification coefficient of 10

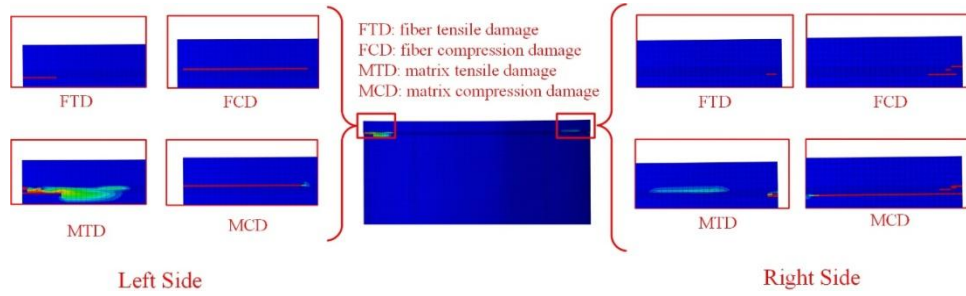


Fig. 16 Damages of the shell by FEM at point E

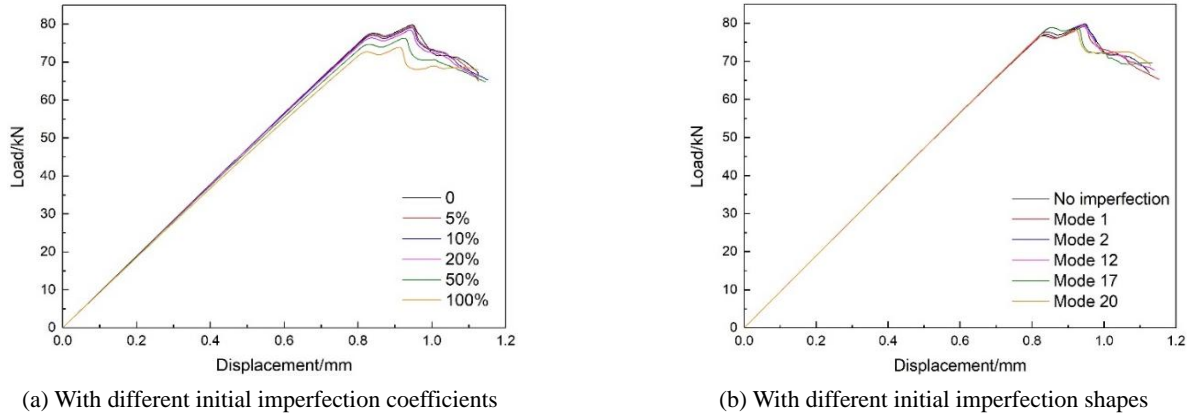


Fig. 17 Load-displacement curves of the shell

and then extend along the circumferential direction. The damages of the shell at point E are shown in Fig. 16, which are consistent with the specimen damages as shown in Fig. 7. Therefore, the validity of the FEM is verified.

4. Discussions

Based on the verified FEM, the effect of the initial geometric imperfections and side supported condition on the buckling and post-buckling behaviors of the shell will be discussed in this section.

4.1 Geometric imperfection sensitivity analysis

A structure is imperfection sensitive if a small variation of imperfection can change the buckling load significantly. The first linear buckling eigenmode with five different imperfection coefficients, including 5%, 10%, 20%, 50% and 100%, are used to study the sensitivity of the 1/3 composite cylindrical shell with an opening to the imperfection magnitudes. Some researchers (Castro *et al.* 2014) discussed the disadvantages of using the first buckling eigenmode for simulating initial geometric imperfections. So two locally deformed eigenmodes (mode 1 and 2) and three globally deformed eigenmodes (mode 12, 17 and 20) with a constant imperfection coefficient of 10% were chosen as the initial geometric imperfections to study the sensitivity to the imperfection shapes. In addition, the shell without imperfection is also analyzed for comparison. The FEM is the same as before.

Fig. 17(a) shows the load-displacement curves of the shell model with different imperfection coefficients, and the corresponding critical buckling loads are listed in Table 3. It can be seen that 6 curves are similar. With imperfection coefficient increasing, the slope and peak load of the curve decreases slightly, but the deviation is very small and negligible. Therefore, imperfection magnitude has little effect on the buckling response and buckling load of the shell.

Fig. 17(b) shows the load-displacement curves of the shell model with different imperfection shapes, and the corresponding critical buckling loads are listed in Table 4. It can be seen that 6 curves are also similar with close buckling loads. The deformations of the shell after collapse corresponding to different imperfection shapes are almost constant as shown in Fig. 18, except that the concavity of the shell with imperfection shape of eigenmode 17 locates at the right upper corner. So different imperfection shape has little effect on the buckling response and buckling load of the shell, even if there is no initial geometric imperfection.

In summary, the buckling response and buckling load of the 1/3 composite cylindrical shell with a central rectangular opening have little dependency upon the geometric imperfection magnitude and shape. The structure is not geometric imperfection sensitive.

4.2 Effect of side supported condition

In the specimen design process, there was an alternative scheme in which the 1/3 composite cylindrical shell was

Table 3 Critical buckling loads of the shell with different imperfection coefficients

Imperfection coefficient	0	5%	10%	20%	50%
Critical buckling load /kN	77.64	77.34	77.01	76.34	74.71

Table 4 Critical buckling loads of the shell with different imperfection shapes

Eigenmode	No imperfection	1	2	12	17
Critical buckling load /kN	77.64	77.01	76.76	78.86	78.83

simply supported by knife-edge constraints along the two sides. So the effect of this kind of side supported condition needs to be studied.

The FEM is the same as before except the side stiffeners is replaced by simply supported constraints ($U_1 = U_2 = 0, UR_1 = UR_2 = 0$ in Fig. 9(b)) along the two sides. The load-displacement curve with this side supported condition is shown in Fig. 19 with a critical buckling load of 77.46 kN which is very close to the result with side stiffeners. This proves that the side supported condition with side stiffeners does not affect the critical buckling load of the shell, but the clamp fixture is simple and the experiment is easier to be carried out in this way.

From Fig. 19, it can be found that the curve slope of the

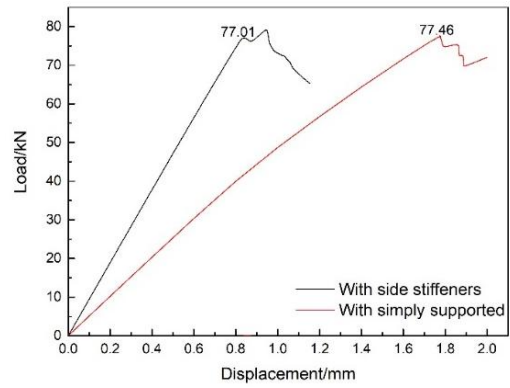


Fig. 19 Load-displacement curves of the shell with side simply supported

shell with side stiffeners is larger, and the shell with simply supported condition has no greater post-buckling load carrying capacity after the critical buckling load. This is because the side stiffeners enhance the axial compressive stiffness of the shell and lead to smaller deformation and damage area in the shell.

Fig. 20 shows the buckling behavior of the cylindrical shell with different side stiffener thickness. It can be found that the side stiffener thickness must be great enough, otherwise the buckling load of the shell decreases. This is because the radial displacements of the side edges are great when the side stiffener thickness is small, as shown in Fig. 21.

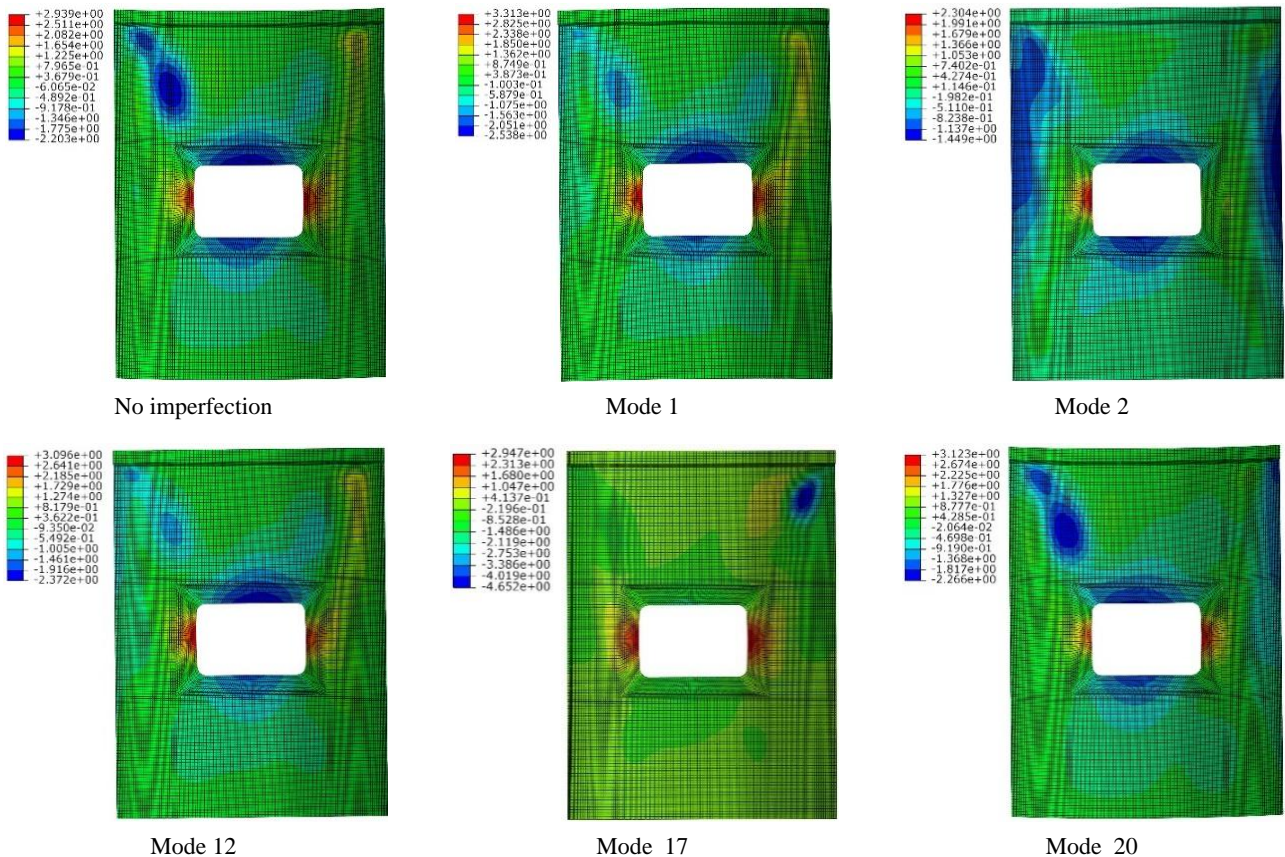


Fig. 18 Deformations of the shell after collapse with different initial imperfection shapes

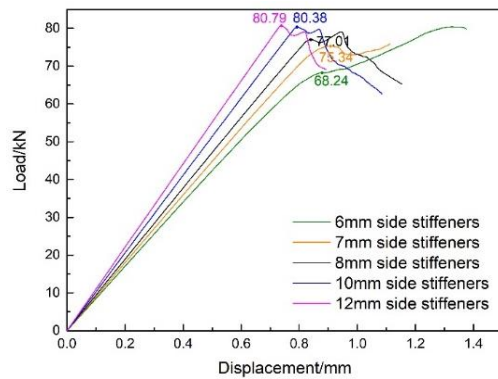


Fig. 20 Effect of the thickness of the side stiffeners

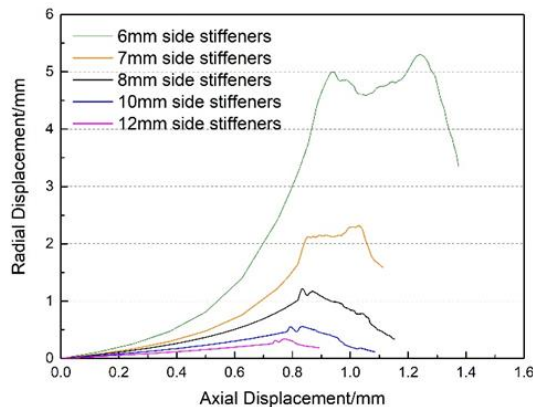


Fig. 21 The radial displacements of the side edge for shells with different side stiffener thickness

5. Conclusions

Studies on the buckling and post-buckling behaviors of a 1/3 composite cylindrical shell with a central rectangular opening were carried out. Based on Newton-Raphson method, a nonlinear FEM with Hashin failure criteria was established and verified by experimental results. Then the geometric imperfection sensitivity and the effect of side supported conditions of the shell were discussed by the FEM. The following conclusions can be obtained:

- The nonlinear analysis based on Newton-Raphson method can be used to investigate the buckling and post-buckling behaviors of the 1/3 composite cylindrical shell with a central rectangular opening relatively accurately. The opening causes stiffness mutation and structural asymmetry, leading to large out-of-plane deformation at a small load. Damages should be considered in the model and can affect the post-buckling behavior of the shell. The linear eigenvalue buckling analysis cannot obtain accurate results.
- The 1/3 composite cylindrical shell with an opening in this paper is not geometric imperfection sensitive. A perfect model can be used to analyze the buckling and post buckling behaviors of the shell.
- The shell with side simply supported by knife-edge

constraints and side stiffeners can provide the same critical buckling load, and the shell with simply supported condition has lower axial compressive structural stiffness and no greater post-buckling load carrying capacity.

References

- Abaqus-inc. (2013), Abaqus User Manual, Version 6.13; Dassault Systemes Simulia Corp., Providence, RI, USA.
- Akbas, S.D. (2017), "Post-buckling responses of functionally graded beams with porosities", *Steel Compos. Struct., Int. J.*, **24**(5), 579-589.
- Altunisik, A.C., Ates, S., Husem, M. and Genc, A.F. (2017), "Collapse of steel cantilever roof of tribune induced by snow loads", *Steel Compos. Struct., Int. J.*, **23**(3), 273-283.
- Aragh, B.S. (2017), "Mathematical modelling of the stability of carbon nanotube-reinforced panels", *Steel Compos. Struct., Int. J.*, **24**(6), 727-740.
- Arbelo, M.A., Kalnins, K., Ozolins, O., Skukis, E., Castro, S.G. and Degenhardt, R. (2015a), "Experimental and numerical estimation of buckling load on unstiffened cylindrical shells using a vibration correlation technique", *Thin-Wall. Struct.*, **94**, 273-279.
- Arbelo, M.A., Herrmann, A., Castro, S.G.P., Khakimova, R., Zimmermann, R. and Degenhardt, R. (2015b), "Investigation of buckling behavior of composite shell structures with cutouts", *Appl. Compos. Mater.*, **22**(6), 623-636.
- Castro, S.G.P., Zimmermann, R., Arbelo, M.A., Khakimova, R., Hilburger, M.W. and Degenhardt, R. (2014), "Geometric imperfections and lower-bound methods used to calculate knock-down factors for axially compressed composite cylindrical shells", *Thin-Wall Struct.*, **74**(1), 118-132.
- Degenhardt, R., Kling, A., Rohwer, K., Orifici, A.C. and Thomson, R.S. (2008), "Design and analysis of stiffened composite panels including post-buckling and collapse", *Comput. Struct.*, **86**(9), 919-929.
- Dong, J.H., Ma, X., Zhuge, Y. and Mills, J.E. (2017), "Shear buckling analysis of laminated plates on tensionless elastic foundations", *Steel Compos. Struct., Int. J.*, **24**(6), 697-709.
- Dubina, D., Ungureanu, V. and Rondal, J. (2005), "Numerical modelling and codification of imperfections for cold-formed steel members analysis", *Steel Compos. Struct., Int. J.*, **5**(6), 515-533.
- Hilburger, M.W. and Starnes, J.H. (2002), "Effects of imperfections on the buckling response of compression-loaded composite shells", *Int. J. Non-Linear Mech.*, **37**(4), 623-643.
- Hilburger, M.W. and Starnes Jr., J.H. (2005), "Buckling behavior of compression-loaded composite cylindrical shells with reinforced cutouts", *Int. J. Non-Linear Mech.*, **40**(7), 1005-1021.
- Hilburger, M.W., Waas, A.M. and Starnes, J.H. (1999), "Response of composite shells with cutouts to internal pressure and compression loads", *AIAA Journal*, **37**(2).
- Hashin, Z. and Rotem, A. (1973), "A fatigue failure criterion for fiber reinforced materials", *J. Compos. Mater.*, **7**(4), 448-464.
- Jabareen, M. (2009), "Rigorous buckling of laminated cylindrical shells", *Thin-Wall. Struct.*, **47**(2), 233-240.
- Jabareen, M. and Sheinman, I. (2006), "Effect of the nonlinear pre-buckling state on the bifurcation point of conical shells", *Int. J. Solids Struct.*, **43**(7), 2146-2159.
- Jabareen, M. and Sheinman, I. (2007), "Buckling and sensitivity to imperfection of conical shells under dynamic step-loading", *J. Appl. Mech.*, **74**(1), 74-80.
- Jullien, J.F. and Limam, A. (1998), "Effects of openings of the

- buckling of cylindrical shells subjected to axial compression”, *Thin-Wall. Struct.*, **31**(1), 187-202.
- Knight, N.F. and Starnes, J.H. (1985), “Postbuckling behavior of axially compressed graphite-epoxy cylindrical panels with circular holes”, *J. Press. Vessel Technol.*, **107**(4), 394-402.
- Lanzi, L. and Giavotto, V. (2006), “Post-buckling optimization of composite stiffened panels: Computations and experiments”, *Compos. Struct.*, **73**(2), 208-220.
- Li, Z.M. and Qiao, P. (2015), “Buckling and postbuckling of anisotropic laminated cylindrical shells under combined external pressure and axial compression in thermal environments”, *Compos. Struct.*, **119**, 709-726.
- Li, Y.W., Elishakoff, I. and Starnes, J.H. (1995), “Axial buckling of composite cylindrical shells with periodic thickness variation”, *Comput. Struct.*, **56**(1), 65-74.
- Li, Z.H., Cheng, X.Q., Wang, Y.L., Yang, K. and Xu, Y.H. (2011), “Compressive properties analysis of composite cylindrical shells”, *Acta Materiae Compositae Sinica*, **28**(1), 206-210.
- Mahmoud, S.R. and Tounsi, A. (2017), “A new shear deformation plate theory with stretching effect for buckling analysis of functionally graded sandwich plates”, *Steel Compos. Struct., Int. J.*, **24**(5), 569-578.
- Orifici, A.C., Thomson, R.S., Herszberg, I., Weller, T., Degenhardt, R. and Bayandor, J. (2008a), “An analysis methodology for failure in postbuckling skin-stiffener interfaces”, *Compos. Struct.*, **86**(1), 186-193.
- Orifici, A.C., Thomson, R.S., Degenhardt, R., Kling, A., Rohwer, K. and Bayandor, J. (2008b), “Degradation investigation in a postbuckling composite stiffened fuselage panel”, *Compos. Struct.*, **82**(2), 217-224.
- Reddy, S.S., Yuvraj, C. and Rao, K.P. (2015), “Design, analysis, fabrication and testing of CFRP with CNF composite cylinder for space applications”, *Int. J. Compos. Mater.*, **5**(5), 102-128.
- Sheinman, I. and Jabareen, M. (2005), “Postbuckling of laminated cylindrical shells in different formulations”, *AIAA Journal*, **43**(5), 1117-1123.
- Shokravi, M. (2017), “Buckling of sandwich plates with FG-CNT-reinforced layers resting on orthotropic elastic medium using Reddy plate theory”, *Steel Compos. Struct., Int. J.*, **23**(6), 623-631.
- Spagnoli, A. and Chryssanthopoulos, M.K. (1999), “Elastic buckling and postbuckling behaviour of widely-stiffened conical shells under axial compression”, *Eng. Struct.*, **21**(9), 845-855.
- Tafreshi, A. (2002), “Buckling and post-buckling analysis of composite cylindrical shells with cutouts subjected to internal pressure and axial compression loads”, *Int. J. Press. Vessels Piping*, **79**(5), 351-359.
- Taheri-Behrooz, F., Omid, M. and Shokrieh, M.M. (2017), “Experimental and numerical investigation of buckling behavior of composite cylinders with cutout”, *Thin-Wall. Struct.*, **116**, 136-144.
- Wu, P.F., Cheng, X.Q., Zhang, J.K., Zhang, T. and Xu, Y.H. (2014), “Effect of opening and boundary conditions on compressive buckling properties of composite one-third cylindrical shell”, *Acta Materiae Compositae Sinica*, **31**(6), 1525-1531.
- Yan, C.N., Fan, Z., Cheng, X.Q. and Li, Z.H. (2012), “Compressive behaviour of composite cylindrical shell with open hole”, *J. Beijing Univ. Aeronaut. Astronaut.*, **38**(7), 920-924.
- Ye, J.R., Yue, G.Q., Zhang, B.M., Lu, S. and Cheng, K. (2011), “Experimental and numerical study of tool effect on curing deformation for the composite missile structure”, *Polym. Polym. Compos.*, **19**(4), 259-264.